Environmental Science
Processes & Impacts

PAPER

Cite this: *Environ. Sci.: Processes Impacts*, 2014, **16**, 858

Photodegradation routes of the herbicide bromoxynil in solution and sorbed on silica nanoparticles†

Juan P. Escalada,[a] Valeria B. Arce,[b] Luciano Carlos,[b] Gabriela V. Porcal,[c] M. Alicia Biasutti,[c] Susana Criado,[c] Norman A. García[c] and Daniel O. Mártire*[b]

Received 31st October 2013
Accepted 17th December 2013

DOI: 10.1039/c3em00576c

rsc.li/process-impacts

Some organic contaminants dissolved in natural waters tend to adsorb on suspended particles and sediments. In order to mimic the photodegradation routes in natural waters of bromoxynil (BXN) adsorbed on silica, we here prepare and characterize silica nanoparticles modified with BXN (NP-BXN). We measure the direct photolysis quantum yield of aqueous BXN at 307 nm (0.064 ± 0.001) and detect the formation of bromide ions as a reaction product. Under similar conditions the photolysis quantum yield of BXN bonded to NP-BXN is much lower (0.0021 ± 0.0004) and does not lead to formation of bromide ions. The rate constant of the reaction of NP-BXN with the excited triplet states of riboflavin, a molecule employed as a proxy of chromophore dissolved organic matter (DOM) was measured in laser flash-photolysis experiments. The rate constants for the overall (k_t) and chemical interaction (k_r) of singlet oxygen with NP-BXN were also measured. Kinetic computer simulations show that the relevance of the direct and indirect (through reactions with reactive species generated in photoinduced processes) photodegradation routes of BXN is very much affected by sorption on silica. Immobilization of the herbicide on the particles, on one hand, affects the photolysis mechanism and lowers its photolysis quantum yield. On the other hand, the results obtained in aqueous suspensions indicate that immobilization also lowers the rate of collisional encounter, which affects the quenching rate constants of excited triplet states and singlet oxygen with the herbicide.

Environmental impact

The herbicide bromoxynil (BXN) absorbs light from the solar radiation reaching the Earth's surface. Thus, its degradation by direct photolysis might be relevant if exposed to sunlight. Additionally, natural waters contain low steady-state concentrations of radicals (carbonate and hydroxyl) and excited states (triplet states of chromophore dissolved organic matter and singlet oxygen), which are formed in photoinduced processes. The reactions of these species with organic contaminants, such as BXN, lead to its photodegradation (indirect photolysis). We here evaluate *in vitro* the relevance of the different photodegradation routes of BXN both dissolved in aqueous solution and in suspensions of silica nanoparticles modified with BXN.

Introduction

Organic pesticides comprise the largest group of xenobiotic compounds deliberately introduced into the environment. These substances are active ingredients in various formulations used for controlling plants, insects and fungi in agriculture, orchards, and public areas. In particular, pesticides used to inhibit the growth of plants, especially weeds, are called herbicides.

The compound 3,5-dibromo-4-hydroxybenzonitrile (bromoxynil, BXN) is a phenolic benzonitrile-based herbicide used for the control of broad-leaved weeds in grain crops, which is intensely used worldwide. This herbicide mimics auxin, the plant growth regulator that promotes unregulated plant growth, which eventually leads to plant death.[1]

The heptanoate, butyrate, and mainly octanoate esters of BXN are also employed for the same purposes. In aqueous medium the esters hydrolyze to yield BXN and the corresponding free carboxylate. The reported hydrolysis half-life of BXN octanoate in sterile solutions of pH 9 is 2.6 days, whereas that in sterile pond water is only 0.5 days.[2] BXN is classified as group C possible human carcinogen and has relatively high toxic effects on aquatic organisms. In addition, it is considered to be developmentally toxic.[3]

[a]*Unidad Académica Río Gallegos de la Universidad Nacional de la Patagonia Austral, 9400 Río Gallegos, Argentina*

[b]*Instituto de Investigaciones Fisicoquímicas Teóricas y Aplicadas (INIFTA), CCT-La Plata-CONICET, Universidad Nacional de La Plata, Diag 113 y 64, 1900 La Plata, Argentina. E-mail: dmartire@inifta.unlp.edu.ar*

[c]*Departamento de Química, Universidad Nacional de Río Cuarto, Campus Universitario, Río Cuarto, Argentina*

† Electronic supplementary information (ESI) available. FTIR of BXN and NP-BXN (table and figure). Details of the characterization methods. Derivation of eqn (6). Calculation of k_a. See DOI: 10.1039/c3em00576c

During the last few decades there has been an increased frequency of pesticide detection in ground and surface waters in Europe[4] and the United States.[5] Traces of BXN of *ca.* 10 ng L^{-1} were detected in surface waters of ponds[6] and the mean annual calculated concentration of BXN in drinking waters from the northern Great Plains of North America is 1 ng L^{-1}.[7]

Generally, abiotic degradation of BXN in soils and subsurface sediments is of minor importance compared to biodegradation.[8] However, since BXN absorbs UV-A light its degradation by photolysis might be relevant if exposed to sunlight, *e.g.*, immediately after application of the herbicide when it is located on the surface of plants or soil. Photodegradation should also be relevant when BXN is present in surface waters either dissolved or sorbed on suspended particles. In aqueous medium the quantum yield of direct photolysis for BXN degradation was found to depend on pH.[9]

The presence of dissolved organic matter (DOM) in natural waters also has an important influence on the light-induced transformation pathways of organic contaminants. On one hand, photolysis of DOM, nitrate and nitrite ions, and various Fe(III) species, leads to the formation of several primary and secondary reactive species.[10] As a result, low steady-state concentrations of radicals (hydroxyl $HO^{\bullet}$ and carbonate $CO_3^{\bullet-}$) and excited states (triplet states of DOM, ^{3}DOM*, and singlet oxygen, $O_2(^1\Delta_g)$) present in the natural waters are able to initiate the oxidation of contaminants, such as BXN. On the other hand, DOM can also contribute to the decrease of the phototransformation rate of contaminants by scavenging of reactive species and screening of the photochemically active light. Zeng and Arnold[11] have recently studied the photodegradation kinetics of sixteen pesticides in natural surface water samples under simulated and natural sunlight. These authors found that for pesticides that were inefficiently degraded by direct photolysis, indirect photolysis induced by $HO^{\bullet}$, $CO_3^{\bullet-}$, $O_2(^1\Delta_g)$ or ^{3}DOM* was the main dissipation process, with $O_2(^1\Delta_g)$ or ^{3}DOM* dominating.

Due to the low solubility of BXN in water (72 mg L^{-1}), it is proposed that the herbicide is rapidly adsorbed on to soil particles.[12] Since silica is a material widely present in soils and suspended in natural waters[13] and BXN is known to adsorb on silica,[14] it is very likely that BXN in natural waters will sorb on suspended silica particles.

The aim of this work is to evaluate the effect of BXN adsorption on its different photodegradation routes relevant in aquatic photochemistry. For this purpose, silica nanoparticles modified with BXN (NP-BXN) were prepared according to reaction (1).

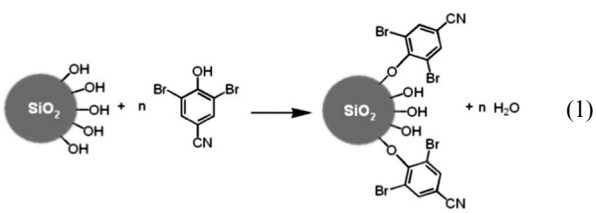

(1)

where n is the number of BXN attached to one silica nanoparticle. The particles were characterized by several techniques: thermogravimetry (TG), Brunauer–Emmett–Teller (BET) analysis, Fourier transform infrared (FTIR), UV-visible spectroscopies and dynamic light scattering (DLS). The particles were chemically modified with BXN to ensure immobilization of the herbicide.

In order to obtain information useful for the estimation of the role of the different photodegradation pathways of BXN in natural waters, time-resolved and steady-state photochemical laboratory experiments were conducted to investigate the photolysis of BXN and NP-BXN, and the interaction of suspensions of NP-BXN with $O_2(^1\Delta_g)$ and the excited states of riboflavin (Rf). Rf is a natural pigment present in all types of natural waters. Although it is part of chromophore dissolved organic matter (DOM), the study of Rf separately allows knowledge in detail of the involved photochemical processes. This vitamin allows the unambiguous measurement of the rate constants of the interaction of its excited triplet states with different substrates by employment of the flash-photolysis technique because the lowest triplet state of Rf and its reduced radical are very well characterized.[15] For these reasons, we employ here Rf as a proxy of chromophore dissolved organic matter (DOM). This was already done previously.[16] The results obtained with NP-BXN are compared to reported data[15] on the quenching of the same excited states by BXN in solution. The basic information obtained here was used to simulate the photodegradation routes of BXN free and chemisorbed on silica particles.

Materials and methods

Materials

$CaCl_2$, BXN, deuterium oxide (D_2O), deuterated methanol (MeOD), riboflavin (Rf), furfuryl alcohol (FFA), catalase (CAT) and superoxide dismutase (SOD) (all from Sigma-Aldrich), ethyl acetate (Ciccarelli, p.a.), K_2HPO_4 and KH_2PO_4 (Merck), rose bengal (RB) and sodium azide (NaN_3) (Anedra), methanol (MeOH) and 2-propanol (Sintorgan), and CaH_2 (Fluka) were used without further purification.

Synthesis and characterization of NP-BXN

For the synthesis of NP-BXN a variation of the condensation method[17,18] was employed (reaction (1)). To a suspension of 1.0 g of silica (Sigma, particle diameter = 7 nm, estimated from the specific surface area (SSA = 390 ± 40 m^2 g^{-1})) in 180 mL *o*-xylene (Aldrich, previously distilled onto molecular sieves), 0.5 g of BXN was added. A continuous solid liquid extractor containing CaH_2 and a condenser with a $CaCl_2$ drying tube was mounted on the reaction flask, and the mixture was refluxed for 24 h. The products were filtered through 20 nm nylon filters, washed with 50 mL hot *o*-xylene and finally with 50 mL ethyl acetate. Samples were dried at 0.1 Torr and at room temperature for 3 h and then at 120 °C for 5 h.

The experimental details of the particle characterization are given in the ESI.†

Photochemical experiments

To reduce colloidal aggregation the aqueous suspensions of the nanoparticles were buffered with a mixture of K_2HPO_4 and

KH_2PO_4 (pH = 6.4).[19] Before the experiments the suspensions were sonicated for 15 min. The steady-state irradiation experiments were performed under stirring.

The quantum yield of direct photolysis (Φ) of BXN and NP-BXN was obtained from eqn (2) by employing a Rayonet lamp as an excitation source. The emission of the lamp presents a bandwidth of about 30 nm and is centered at 307 nm.

$$\Phi = \frac{R}{P_0(1 - 10^{-az})} \quad (2)$$

In eqn (2) R is the initial rate of BXN or NP-BXN degradation, a is the solution absorption coefficient (cm^{-1}) and z is the optical pathlength (cm). The incident photon rate (P_0), measured using potassium ferrioxalate as actinometer,[20] was 2.88×10^{-6} Einstein s^{-1} L^{-1}.

For measuring the quantum yield of direct photolysis quantification of free BXN was performed by HPLC using a Shimadzu CMB-20A instrument (solvent delivery module LC-20AT, on-line degasser DGU-20A5, UV-vis photodiode array detector SPD-M20A, column oven CTO-10 A5 VP and autosampler SIL-20AAT) equipped with a Lichrospher column (RP-C18, 4 mm i.d. × 125 mm long). The column temperature was maintained at 25 °C. Elution conditions: mobile phase composed of 40/60 v/v acetonitrile and an aqueous solution ($[H_3PO_4] = 0.01$ M); flow rate: 1 mL min^{-1}. The detection wavelength was 220 nm. For the quantum yield measurements, quantification of sorbed BXN was carried out by UV-visible spectroscopy. To obtain the absorbance of the bonded herbicide the fitting function of the scattering c/λ^n (with c and n constants) obtained over the wavelength range 400–700 nm was extrapolated to shorter wavelengths and subtracted from the optical density spectra of the NP-BXN suspensions.[19]

An ICMetrohm 881 instrument equipped with a Metrosep A Supp 5 column (150 mm length and 4 mm i.d.) was employed for the ionic chromatographic measurements of bromide ions. The mobile phase was an aqueous solution containing 1 mM $NaCO_3H$ plus 3.2 mM K_2CO_3. The flow rate was 0.7 mL min^{-1}.

Fluorescence lifetimes were measured on an Edinburgh FL-9000CD instrument with the time-correlated single photon counting technique (SPC). Excitation and emission wavelengths for Rf were 445 and 515 nm, respectively. The measurements were performed with solutions of Rf ($A^{445} = 0.23$) in aqueous K_2HPO_4/KH_2PO_4 buffer of pH = 6.4 containing (0–2.5 g L^{-1}) NP-BXN suspended in the solution.

Steady-state measurements of the fluorescence anisotropy $\langle r \rangle$ were performed with a Hitachi 2500 spectrofluorometer, with Glan–Thomson polarizers. Fluorescence anisotropy values were obtained from eqn (3).

$$\langle r \rangle = \frac{I_{VV} - GI_{VH}}{I_{VV} + 2GI_{VH}} \quad (3)$$

where G is the sensitivity factor of the detection system; I_{VV} and I_{VH} are the vertically and horizontally polarized emission components after excitation by vertically polarized light. All measurements were carried out at 25 °C.

Laser Flash-Photolysis (LFP) experiments were performed using instrumentation that has been described previously.[21] For the experiments Ar-saturated NP-BXN suspensions in Rf solutions in either methanol or buffered aqueous solutions were employed.

Rose Bengal ($A^{532} = 0.33$) was used as the sensitizer in all the $O_2(^1\Delta_g)$ quenching assays. NP-BXN concentrations < 0.2 g L^{-1} suspended in MeOD or buffered D_2O were employed. To measure the overall quenching rate constant, k_t, for the deactivation of $O_2(^1\Delta_g)$ by NP-BXN the excitation source was the second harmonic of a Nd:YAG SL400 Spectron Laser. The detection and acquisition systems have been described elsewhere.[22]

To measure the rate constant k_r for the chemical reaction of $O_2(^1\Delta_g)$ with NP-BXN comparative continuous irradiation experiments of aqueous solutions containing the sensitizer and a concentration of 0.5 mM of the substrates (FFA or BXN bonded to NP-BXN) with a 150 W quartz halogen lamp (>350 nm, cut-off filter) were performed. Under these conditions, the pseudo first-order slope for the consumption of oxygen is proportional to k_r. The value of k_r for FFA employed in the calculations was 1.2×10^8 M^{-1} s^{-1}.[23] The participation of photogenerated ROS was tested by comparing the rates of oxygen consumption in the presence and absence of specific scavengers for Rf-sensitized photolysis of NP-BXN. The oxygen concentration was measured with an oxygen-sensitive electrode (Orion 97-0899).

Results

Characterization of NP-BXN

From the DLS measurements (Table 1), we can conclude that the 7 nm diameter particles are aggregated. The percentage of organic groups (%OG = 19%) for NP-BXN was estimated from the loss of mass observed over the range 200 to 700 C in the TG analysis. We here also observe a decrease in specific surface area upon silica functionalization with the organic groups, as already reported for different systems.[16]

The average mass of a spherical 7 nm diameter bare SiO_2 nanoparticle calculated from the volume of the nanoparticle and the density of silica (2200 kg m^3)[24] is 3.95×10^{-19} g. From the percentage of organic groups bonded to the particle (19%, see Table 1), a calculated typical number "n" of organic groups in a single particle is 160. The bare SiO_2 particles contain in average 708 surface silanol groups[17] which means that *ca.* 23% of them are modified with the pesticide.

The FTIR spectrum of NP-BXN shows additional peaks compared to that of the bare silica nanoparticles (Table S1 and Fig. S1 in the ESI†). These peaks are also present in the spectrum of BXN. The peaks in the region from 3000 to 2800 cm^{-1}

Table 1 Results of NP-BXN characterization

Technique	Parameter	
DLS	Hydrodynamic diameter (nm) and full width at half maxima (FWHM)	176 ± 234 2111 ± 1463
BET	S_{BET} (m^2 g^{-1})	260.1 ± 0.8
TG	%OG (w/w)	19.0%

are assigned to the CH_2 stretching.[25] Those in the range from 1600 to 1475 cm^{-1} are due to the –C=C– stretching in the ring. In particular, the peak at 2233.7 cm^{-1} is attributed to the CN group. Any absorption due to the vibration modes assigned to the Si–O–C moiety is masked by the strong Si–O–Si absorption signals at 1100 cm^{-1}.[25]

Direct photolysis of BXN and NP-BXN

Kochany *et al.*[26] investigated the photochemistry of the herbicide BXN in 0.05 mM solutions by irradiating at $\lambda \sim 313$ nm. The measured photolysis quantum yields were 0.008, 0.048, and 0.044 at pH 2.6, 7.0, and 11.0, respectively. These authors detected 3-bromo-4-hydroxybenzonitrile and 4-hydroxybenzonitrile as products of hydrogenation, where one or two H atoms are substituted for the Br atoms. In a later study, Guitonneau *et al.*[27] reported a photolysis quantum yield for BXN at pH = 7 of 0.02 at two different wavelengths, 254 and 290 nm. The products identified by these authors upon irradiation at $\lambda =$ 254 nm were 4-hydroxybenzonitrile and the hydroxylation products 5-bromo-3,4-dihydroxybenzonitrile (DHBN, also found by Machado *et al.*[28] by irradiation at 296 nm) and 3,4,5-trihydroxybenzonitrile (THBN).

Formation of hydroxylation products should be accompanied by generation of bromide ions, although this was not studied.

We here measure the decay of BXN upon irradiation of a 10 μM solution (pH = 7.0) of the pesticide at (307 ± 30) nm. The decay of BXN detected by HPLC is shown in Fig. 1. The [BXN] follows a pseudo-first order kinetics with an apparent rate constant (k_{app}) of (0.28 ± 0.02) min^{-1}. From these experiments a quantum yield of 0.064 ± 0.001 at 307 nm is obtained (using eqn (2)). This value is very close to that reported by Kochany *et al.*[26] For suspensions of NP-BXN (pH = 7.0) the quantum yield estimated from the changes in the UV-visible absorption spectrum at short irradiation times is 0.0021 ± 0.0004.

Irradiation of the BXN solution leads to the formation of bromide ions (see Fig. 1). To account for this observation the reaction sequence shown in Scheme 1 is proposed. This

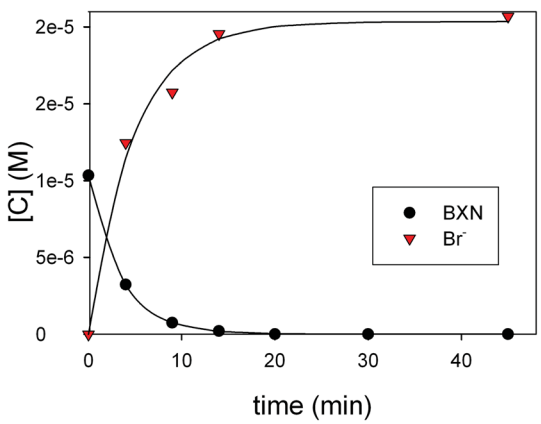

Fig. 1 Evolution of [BXN] and [Br^-] upon irradiation of a 10 μM solution of BXN of pH = 7.0. The solid lines show the fitting of [BXN] to an exponential decay function and fitting of [Br^-] to eqn (6).

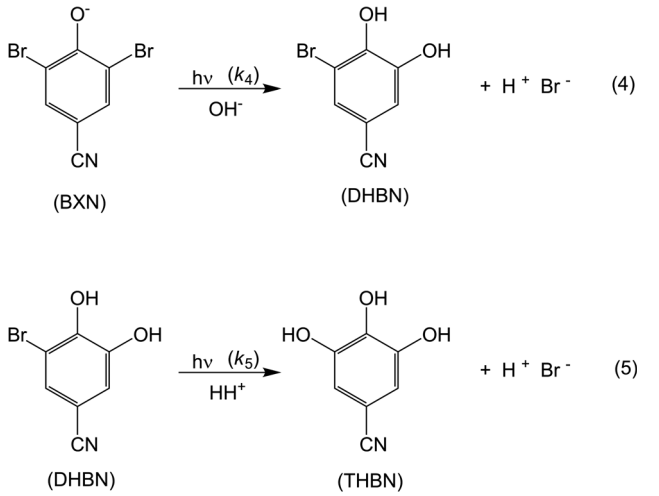

Scheme 1 Proposed reaction sequence for the photolysis of BXN in aqueous solution.

heterolytic mechanism involves in the first step the scissions, probably concerted, of a C–halogen bond and a molecule of water, as previously suggested for chloroxynil and ioxynil.[29] The formation of THBN from DHBN is proposed to take place by a similar reaction route.

As can be seen in Fig. 1, [Br^-] rises up to twice $[BXN]_0$.

If we assume that the second bromide ion is eliminated much faster than the first one, *i.e.*, $k_5 \gg k_4$, resolution of the mechanism shown in Scheme 1 leads to eqn (6) (see ESI†).

$$[Br^-] \approx 2 \times [BXN]_o \times (1 - e^{-k_4 \times t}) \quad (6)$$

The [Br^-] was fitted to eqn (6) (Fig. 1). The value of k_4 obtained from the fitting, (0.20 ± 0.03) min^{-1}, is almost coincident with that of k_{app} = (0.28 ± 0.02) min^{-1} calculated for the decay of [BXN], as expected if the condition $k_5 \gg k_4$ applies.

Bromide ions were analyzed in irradiated 0.015 g L^{-1} suspensions of NP-BXN in pH = 7 aqueous medium. Although the concentration of BXN bonded to the suspended particles in these assays is 10 μM, coincident with that of dissolved BXN in the experiments shown in Fig. 1, no bromide ion generation (detection limit 10^{-7} M) could be detected after 90 min of irradiation. Due to the lower photolysis quantum yield of NP-BXN compared to that of BXN, the experiment was repeated with 0.15 g L^{-1} suspensions of NP-BXN irradiated for 60 min. However, we were also unable to detect bromide ions under these conditions. These results indicate that bonding to NP-BXN, *i.e.*, replacement of the electron donating O^- group for the electron-withdrawing O–Si group affects the direct photolysis route of BXN.

Reactions of NP-BXN with reactive species formed upon irradiation of Rf

The reactivity of the lowest excited singlet states of Rf ($^1Rf^*$) with BXN bonded to the nanoparticles was studied by time-resolved fluorescence spectroscopy. Addition of NP-BXN or bare silica nanoparticles in the concentration range 0–2.5 g L^{-1} to a

solution of Rf did not affect the fluorescence lifetime of the vitamin (τ_F = 4.9 ns). Suspensions with higher amounts of NP-BXN were not employed to avoid precipitation during the fluorescence experiments. We can conclude that the concentration of surface organic groups in the modified particles is too small to affect the fluorescence lifetime of Rf. The measured fluorescence anisotropy $\langle r \rangle = 0.005$ obtained for the 2.5 g L^{-1} suspensions of NP-BXN shows that in freshly prepared solutions Rf is not adsorbed on NP-BXN. Thus, under the conditions of the flash-photolysis experiments performed to investigate reaction (7) between the lowest triplet excited states of Rf (^{3}Rf*) and NP-BXN we will also consider that Rf is free in solution and not sorbed on the nanoparticles.

$$^3\text{Rf}^* + \text{NP-BXN} \rightarrow \text{Rf}^{\bullet -} + \text{NP–BXN}^{\bullet +} \quad (7)$$

The decay of ^{3}Rf* monitored at 670 nm was fitted to single exponential functions both in Ar-saturated aqueous or methanol solutions of the sensitizer. The decays of ^{3}Rf* in Ar-saturated neat aqueous buffer or methanol were not affected by the presence of 2.5 g L^{-1} of suspended bare SiO_2 nanoparticles, which shows that any reaction of ^{3}Rf* with the silanol groups of the particles must be neglected.

From the 20% OG w/w obtained from the TG analysis, the bimolecular rate constant k_7 for the quenching of ^{3}Rf* by the particles (per mole of NP-BXN) in water or methanol suspensions was calculated from the linear plots of τ_T^{-1} *vs.* [BXN] bonded to the particles (see Table 2 and Fig. 2).

The products of reaction (7) in aqueous medium were analyzed from the absorption spectrum taken 20 μs after the laser pulse. The spectrum is similar to that of the semiquinone radical,[30] RfH$^\bullet$, formed by protonation of Rf$^{\bullet -}$. Although it was not possible to observe the absorption of any oxidized product of BXN, NP-BXN$^{\bullet +}$ should be formed as a consequence of the electron transfer process.

The involvement of ROS in the Rf-photosensitized degradation of NP-BXN was evaluated in steady-state experiments through measurements of the oxygen consumption in the presence of specific scavengers (Fig. 3). The participation of $O_2(^1\Delta_g)$ and $O_2^{\bullet -}$ was confirmed by the observed decreased oxygen uptake in the presence of NaN_3 (10 mM) and SOD (1 μg mL^{-1}), respectively, as also reported for the Rf-photosensitized degradation of BXN.[15] The addition of 2-propanol (20 mM) had almost no effect on the rate of oxygen uptake. Thus, the involvement of the hydroxyl radical can be neglected.

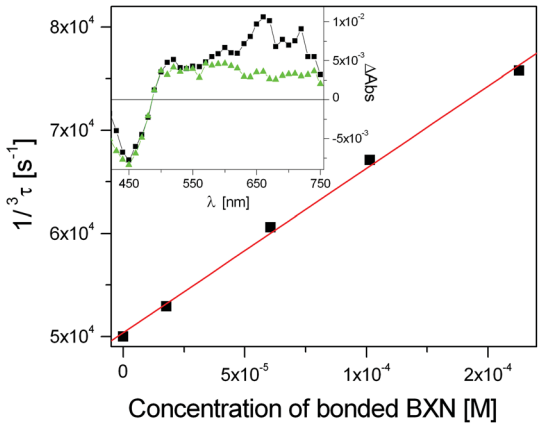

Fig. 2 Plot of the reciprocal of the ^{3}Rf* lifetime *vs.* [BXN] bonded to NP. Inset: transient absorption spectra taken 2 μs after the laser pulse with Rf (A^{355} = 0.2) in Ar-saturated aqueous phosphate buffer in the absence (squares) and presence of 1 g L^{-1} NP-BXN (triangles).

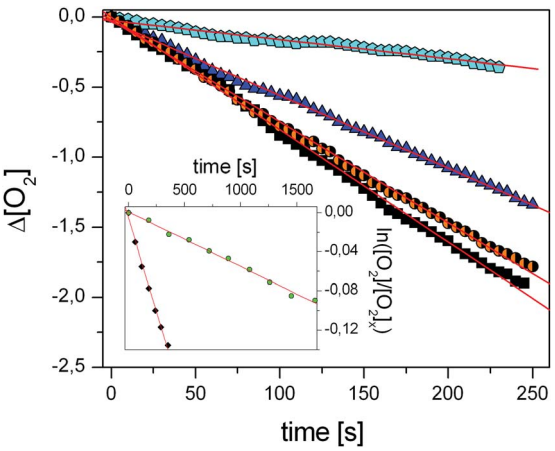

Fig. 3 Oxygen consumption in suspensions of 0.5 g L^{-1} NP-BXN of pH = 6.4 upon riboflavin sensitized photoirradiation containing in the absence (squares) and presence of NaN_3 (0.5 mM) (pentagons), superoxide dismutase (SOD) (1 μg mL^{-1}) (triangles), and in the presence of 2-propanol (circles). Inset: first order plots for oxygen uptake upon Rose Bengal photosensitized oxidation of NP-BXN (0.5 g L^{-1}) (circles) and furfuryl alcohol (0.04 mM) (squares) at pH 6.4.

Deactivation of $O_2(^1\Delta_g)$ by NP-BXN

Scavenging of $O_2(^1\Delta_g)$ by substrates may take place by two main pathways: (1) a chemical reaction with rate constant k_r and (2) a physical interaction with quenching constant k_q. The

Table 2 Quenching rate constants of $O_2(^1\Delta_g)$ and ^{3}Rf* by NP-BXN and BXN[a]

		k_r	k_t	k_7
NP-BXN	H_2O/D_2O	$(2.0 \pm 0.2) \times 10^{6b}$	$(1.2 \pm 0.7) \times 10^{8c}$	$(1.6 \pm 0.5) \times 10^{8b}$
	MeOH/MeOD	$(1.4 \pm 0.3) \times 10^{7d}$	$(2.9 \pm 0.1) \times 10^{7e}$	$(7.3 \pm 0.6) \times 10^{7d}$
BXN	H_2O/D_2O	$1.6 \times 10^{7f,g}$	$2.4 \times 10^{7f,h}$	$(2.6 \pm 0.1) \times 10^{9b}$
	MeOH/MeOD	$2.0 \times 10^{6d,f}$	$4.0 \times 10^{6e,f}$	$2.1 \times 10^{9d,f}$

[a] Values expressed per mole of BXN; k_r and k_t represent the rate constants for the chemical and overall interaction with $O_2(^1\Delta_g)$; k_7 stands here for the rate constant of reaction (7) or for a similar reaction with free BXN. [b] In buffered H_2O (pH = 6.4). [c] In buffered D_2O (pD = 6.4). [d] In unbuffered MeOH. [e] In unbuffered MeOD. [f] From ref. 12. [g] In H_2O (pH = 7). [h] In D_2O (pD = 7).

bimolecular rate constant for the overall process, $k_t = k_q + k_r$, includes the contribution of both interactions.

The decay lifetimes of $O_2(^1\Delta_g)$, τ_0, both in air-saturated D_2O buffer or MeOD were not affected by the presence of 2.5 g L^{-1} of suspended bare SiO_2 nanoparticles, which shows that any reaction of $O_2(^1\Delta_g)$ with the silanol groups of the particles should be negligible. In the presence of NP-BXN the observed lifetime, τ_Δ, decreased with [NP-BXN]. The values of k_t were obtained from the linear plots of τ_Δ^{-1} *vs.* [BXN] bonded to NP-BXN in buffered D_2O (pD = 6.4) or unbuffered MeOD (Fig. 4 and Table 2).

From comparison of the oxygen uptake plots obtained upon irradiation of suspensions of NP-BXN and solutions of FFA in the presence of RB under similar conditions (the inset of Fig. 4), the values of k_r were obtained (Table 2).

Discussion

For comparative purposes Table 2 also shows the rate constants for the reactions of ^{3}Rf* and $O_2(^1\Delta_g)$ with BXN, obtained from ref. 15 under similar conditions.

Immobilizing the quencher at a surface reduces access from solution and lowers the rate of collisional encounter in the absence of adsorption.[17,31] This explains the lower values of k_7 expressed per mole of BXN when the herbicide is bonded to the particles both in buffered aqueous solution and unbuffered methanol (Table 2) because Rf is not expected to be sorbed on NP-BXN (see above). Unexpectedly, the value of k_t obtained here for NP-BXN in D_2O per mole of BXN results higher than that reported for free BXN (Table 2). This could be due to the presence of small amounts of physical quenchers of singlet oxygen as impurity of NP-BXN incorporated during the modification.

The rate constant k_r also decreases when BXN is bonded to NP-BXN in aqueous medium. To explain this result we should consider the negative surface charge of the nanoparticles in aqueous medium due to deprotonation of the silanol groups, which very likely disfavors adsorption of the sensitizer (RB).[32]

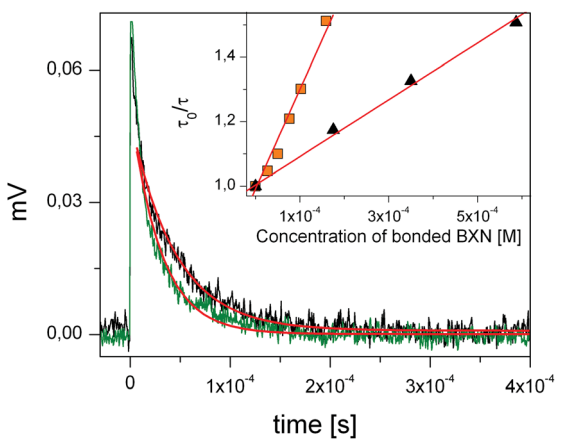

Fig. 4 Phosphorescence decay of $O_2(^1\Delta_g)$ in air-saturated buffered (pD = 6.4) D_2O without (upper signal) and with 0.22 g L^{-1} (lower signal) NP-BXN. Inset: plot of τ_0/τ_Δ *vs.* [BXN] bonded to NP-BXN in D_2O (squares) and MeOD (triangles).

The involvement of the phenol group in the bonding to the particles should also be at least partially responsible for the decrease of the rate constant for the interaction of NP-BXN with $O_2(^1\Delta_g)$ compared to that for the free herbicide. However, chemisorption on the particles produces an enhancement of the values of k_r and k_t in methanol suspensions, which indicates that RB is adsorbed on NP-BXN suspended in the organic solvent.

Computer simulations

Photochemical transformations of pesticides in natural waters are restricted to compartments exposed to sunlight—*e.g.*, the topmost meter(s) of lakes or rivers, which contain low steady-state concentrations of species able to oxidize BXN, such as excited triplet states of dissolved organic matter, ^{3}DOM*, $O_2(^1\Delta_g)$, and HO$^\bullet$ radicals (indirect photolysis).[33] Thus, both direct and indirect photolysis routes of BXN in these environments were considered in the simulations. In order to evaluate the role of the direct and indirect photodegradation routes of BXN and NP-BXN in sunlit natural waters, the following simplified mechanism was considered:

$$HR + h\nu \rightarrow P_8 \quad (8)$$

$$^3DOM^* + HR \rightarrow P_9 \quad (9)$$

$$O_2(^1\Delta_g) + HR \rightarrow P_{10} \quad (10)$$

$$HO^\bullet + HR \rightarrow P_{11} \quad (11)$$

where HR stands for the free (BXN) and sorbed (NP-BXN) herbicide and the product of the reaction is denoted by P_i.

The rate constants of the chemical reaction ($k_{10} = k_r$) of $O_2(^1\Delta_g)$, with BXN and NP-BXN used in the simulations, are taken from Table 2. For the rate constants of reaction (7), we employed those for the reactions of ^{3}Rf* with HR (k_7), *i.e.*, Rf was used as proxy of chromophore DOM.[34] Despite Rf can be employed to simulate DOM, we should keep in mind that in addition to Rf-like substances, other organic molecules with different chemical and photochemical properties are present in natural waters. For BXN the reported value of $k_{11} = 8.45 \times 10^9$ M^{-1} s^{-1} was used.[35] For NP-BXN two values of $k_{11} = 8.45 \times 10^9$ M^{-1} s^{-1} and 8.45×10^8 M^{-1} s^{-1} was used. The latter was chosen to account for the immobilization effect of the scavenger at the surface of the particle, see above.

The average half life $t_{1/2}$ of the herbicide can be obtained from eqn (10).

$$t_{1/2} = \ln 2/(k_9 \times [^3DOM^*]_{SS} + k_{10} \times [O_2(^1\Delta_g)]_{SS} + k_{11} \times [HO^\bullet]_{SS} + k_a \times \Phi) \quad (12)$$

where the subscripts SS are used to denote steady-state concentrations. The average values of $[^3DOM^*]_{ss}$, $[O_2(^1\Delta_g)]_{ss}$, and $[HO^\bullet]_{ss}$ employed in the simulations were 5×10^{-16}, 5×10^{-13}, and 1×10^{-16} M, respectively.[11,36–38] The constant k_a is the specific rate of light absorption and Φ is the photolysis quantum yield (0.064 for BXN and 0.0021 for NP-BXN, see

above). The calculation of $k_a = 7.92 \times 10^{-3}$ considering the reported underwater midday solar irradiance in the wavelength range from 300 to 330 nm is shown in the ESI.†[39]

Eqn (12) shows a drastic effect of sorption on the value of $t_{1/2}$, which is 22 min for free BXN and *ca.* 10 h for NP-BXN.

Resolution of the mechanism given by reactions (8)–(11) leads to eqn (13) and (14) for the concentration of P_8, P_9, P_{10}, and P_{11}.

$$[P_8] = -\frac{(k_a \times \Phi)}{k_S^T} \times \left(e^{-k_S^T \times t} - 1\right) \times [HR]_0 \quad (13)$$

$$[P_j] = -\frac{(k_j \times [OX]_{SS})}{k_S^T} \times \left(e^{-k_S^T \times t} - 1\right) \times [HR]_0 \quad (14)$$

where k_j stands for the rate constants of reactions (9)–(11), $[OX]_{ss}$ represents the steady-state concentration of the corresponding oxidizing species, and k_S^T is given by eqn (15).

$$k_S^T = k_9 \times [^3DOM^*]_{SS} + k_{10} \times [O_2(^1\Delta_g)]_{SS} + k_{11} \times [HO^\bullet]_{SS} + k_a \times \Phi \quad (15)$$

The simulated relative depletion of HR was carried out after 10 h of disposal in the natural water. At this time the depletion of BXN and NP-BXN is more than 99% and *ca.* 63%, respectively.

The main photochemical route of the herbicide consumption either free in solution or sorbed on the particles is through direct photolysis. For BXN, *ca.* 98% of the photodegradation products correspond to the direct photolysis route. For NP-BXN the simulations with $k_{11} = 8.45 \times 10^9$ M^{-1} s^{-1} and 8.45×10^8 M^{-1} s^{-1} show that direct photolysis is responsible for 89 and 93% of the herbicide degradation, respectively. Fig. 5 shows the relative amount of BXN depleted by indirect photoprocesses at $t = 10$ h for BXN and NP-BXN. As can be seen in the figure, the main indirect photochemical sink of the herbicide is through reaction with $O_2(^1\Delta_g)$. For the free herbicide the simulated relative contributions of the ^{3}DOM* and $HO^\bullet$ pathways are similar. This is also the case for NP-BXN when the simulation is done with the lower value of k_{11}, which seems more realistic because immobilization of the quencher at a surface reduces access from solution and lowers the rate of collisional encounter.[17,31]

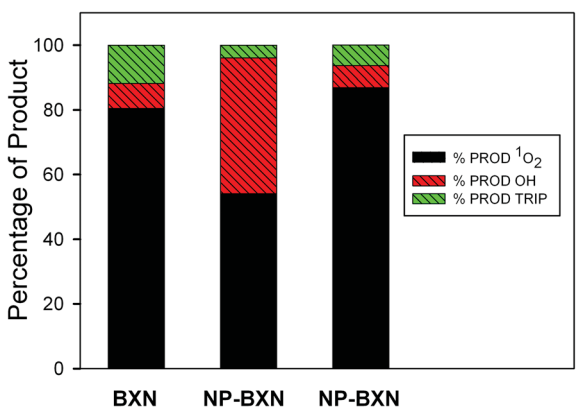

Fig. 5 Simulated BXN and NP-BXN degradation after 10 h and 50 h, respectively. The simulation in the middle was obtained taking $k_{11} = 8.45 \times 10^9$ M^{-1} s^{-1} and that on the right with $k_{11} = 8.45 \times 10^8$ M^{-1} s^{-1}.

Conclusions

Immobilization of the herbicide on the particles, on one hand, affects the photolysis mechanism and lowers its photolysis quantum yield. On the other hand, as expected, the results obtained in aqueous suspensions indicate that immobilization also lowers the rate of collisional encounter, which affects the quenching rate constants of excited triplet states and singlet oxygen with the herbicide.

Computer simulations of the photochemical fate of the herbicide in sunlit natural waters show that the main route of bromoxynil consumption either free in solution or sorbed on the particles is through direct photolysis. The second photochemical sink is through reaction with singlet oxygen.

Abbreviations

%OG	Percentage of organic groups
$\langle r \rangle$	Fluorescence anisotropy
^{1}Rf*	Excited singlet states of Rf
^{3}DOM*	Triplet states of DOM
^{3}Rf*	Triplet states of Rf
BET	Brunauer–Emmett–Teller analysis
BXN	Bromoxynil
CAT	Catalase
$CO_3^{\bullet -}$	Radical carbonate
DHBN	5-Bromo-3,4-dihydroxybenzonitrile
DLS	Dynamic light scattering
DOM	Dissolved organic matter
FFA	Furfuryl alcohol
FTIR	Fourier transform infrared spectroscopy
$HO^\bullet$	Hydroxyl radical
HPLC	High pressure liquid chromatography
HR	Herbicide (BXN or NP-BXN)
k_{app}	Apparent rate constant
k_q	Quenching constant for the physical interaction singlet oxygen with NP-BXN or BXN
k_r	Rate constants for the chemical interaction singlet oxygen with NP-BXN or BXN
k_t	Rate constants for the overall interaction singlet oxygen with NP-BXN or BXN
LFP	Laser Flash-Photolysis
NP-BXN	BXN bonded to silica nanoparticles
$O_2(^1\Delta_g)$	Singlet oxygen
$O_2^{\bullet -}$	Superoxide radical anion
RB	Rose Bengal
Rf	Riboflavin
$Rf^{\bullet -}$	Riboflavin radical anion
$RfH^\bullet$	Semiquinone radical
ROS	Reactive oxygen species
SOD	Superoxide dismutase
SPC	Single photon counting technique
TG	Thermogravimetry
THBN	3,4,5-Trihydroxybenzonitrile.

Acknowledgements

This research was supported by ANPCyT, Argentina (PICT 2008 # 00686), and CIC (Buenos Aires, Argentina). J.P.E. thanks CONICET (Argentina) for a post-doctoral fellowship. L.C., G.V.P., M.A.B., S.C., and N.A.G. are researchers from CONICET. V.B.A. and D.O.M. are researchers from CIC. The reviewers are also thanked for their constructive input.

Notes and references

1 Saskatchewan Ministry of Agriculture, *Guide to Crop Protection*, Saskatchewan, Regina, SK, Canada, 2008.
2 D. C. G. Muir, D. F. Kenny, N. P. Grift, R. D. Robinson, R. D. Titman and H. R. Murkin, *Environ. Toxicol. Chem.*, 1991, **10**, 395–406.
3 U.S. EPA, 1998. Pesticide Reregistration – Bromoxynil. U.S. Environmental Protection Agency EPA-738-R-98–013. U.S.A., http://www.epa.gov.
4 European Environment Agency, Hazardous substances in Europe's fresh and marine waters, An overview: EEA Technical report No. 8/2011.
5 J. E. Barbash, G. P. Thelin, D. W. Kolpin and R. J. Gilliom, *J. Environ. Qual.*, 2001, **30**, 831–845.
6 P. G. Messing, A. Farenhorst, D. T. Waite, D. A. R. McQueen, J. F. Sproull, D. A. Humphries and L. L. Thompson, *Atmos. Environ.*, 2011, **45**, 7227–7234.
7 D. B. Donald, A. J. Cessna, E. Sverko and N. E. Glozier, *Environ. Health Perspect.*, 2007, **115**, 1183–1191.
8 M. S. Holtze, S. R. Sørensen, J. Sørensen and J. Aamand, *Environ. Pollut.*, 2008, **154**, 155–168.
9 P. Chelme-Ayala, M. G. El-Din and D. W. Smith, *Water Res.*, 2010, **44**, 2221–2228.
10 J. Wenk, U. von Gunten and S. Canonica, *Environ. Sci. Technol.*, 2011, **45**, 1334–1340.
11 T. Zeng and W. A. Arnold, *Environ. Sci. Technol.*, 2013, **47**(13), 6735–6745.
12 http://www.nufarm.co.nz/Assets/18500/1/EmblemFloSDS0911.pdf.
13 W. Clymans, G. Govers, B. Van Wesemael, P. Meire and E. Struyf, *Geoderma*, 2011, **167–168**, 228–235.
14 W. Palm, M. Millet and C. Zetzsch, *Ecotoxicol. Environ. Saf.*, 1998, **41**, 36–43.
15 J. P. Escalada, A. Pajares, J. Gianotti, A. Biasutti, S. Criado, P. Molina, W. Massad, F. Amat-Guerri and N. A. Garcia, *J. Hazard. Mater.*, 2011, **186**, 466–472.
16 D. Vione, P. R. Maddigapu, E. De Laurentiis, M. Minella, M. Pazzi, V. Maurino, C. Minero, S. Kouras and C. Richard, *Water Res.*, 2011, **45**, 6725–6736.
17 V. B. Arce, S. G. Bertolotti, F. J. V. E. Oliveira, C. Airoldi, M. C. Gonzalez, P. E. Allegretti and D. O. Mártire, *J. Phys. Chem. C*, 2011, **115**, 18122–18130.
18 G. C. Ossenkamp, T. Kemmitt and J. H. Johnston, *Langmuir*, 2002, **18**, 5749–5754.
19 A. E. Ruiz, P. Caregnato, V. B. Arce, M. M. Schiavoni, V. C. Mora, M. C. Gonzalez, P. E. Allegretti and D. O. Mártire, *J. Phys. Chem. C*, 2007, **111**, 7623–7628.
20 L. Carlos, M. Cipollone, D. B. Soria, S. Moreno, P. R. Ogilby, F. S. GarcíaEinschlag and D. O. Mártire, *Sep. Purif. Technol.*, 2012, **91**, 23–29.
21 E. Haggi, S. Bertolotti and N. A. García, *Chemosphere*, 2004, **55**, 1501–1507.
22 S. Criado, S. G. Bertolotti and N. A. García, *J. Photochem. Photobiol., B*, 1996, **34**, 79–86.
23 P. G. Tratniek and J. Hoigné, *Environ. Sci. Technol.*, 1991, **25**, 1956–1964.
24 H. K. Kammler, G. Beaucage, R. Mueller and S. E. Pratsinis, *Langmuir*, 2004, **20**, 1915–1921.
25 M. J. Llansola Portolés, F. Rodríguez Nieto, D. B. Soria, J. I. Amalvy, P. J. Peruzzo, D. O. Mártire, M. O. Kotler, O. Holub and M. C. Gonzalez, *J. Phys. Chem. C*, 2009, **113**, 13694–13702.
26 J. Kochany, G. GhausChoudhry and G. R. Barrie Webster, *Pestic. Sci.*, 1990, **28**, 69–81.
27 S. Guitonneau, S. Momege, A. Schafmeier, P. O. Viac and P. Meallier, *Rev. Sci. Eau*, 1995, **8**, 201–216.
28 F. Machado, L. Collin and P. Boule, *Pestic. Sci.*, 1995, **45**, 107–110.
29 M. A. Malouki, A. Zertal, B. Lavédrine, T. Sehili and P. Boule, *J. Photochem. Photobiol., A*, 2004, **168**, 15–22.
30 C. Lu, C. G. Bucher and W. Sander, *ChemPhysChem*, 2004, **5**, 47–56.
31 R. D. Astumian and Z. A. Schelly, *J. Am. Chem. Soc.*, 1984, **106**, 304–308.
32 S. Ong, X. Zhao and K. B. Eisenthal, *Chem. Phys. Lett.*, 1992, **191**, 327–335.
33 K. Fenner, S. Canonica, L. P. Wackett and M. Elsner, *Science*, 2013, **341**, 752–758.
34 D. Vione, P. R. Maddigapu, E. De Laurentiis, M. Minella, M. Pazzi, V. Maurino, C. Minero, S. Kouras and C. Richard, *Water Res.*, 2011, **45**, 6725–6736.
35 P. Chelme-Ayala, M. G. El-Din and D. W. Smith, *Chemosphere*, 2010, **78**, 557–562.
36 R. G. Zepp and D. M. Cline, *Environ. Sci. Technol.*, 1977, **11**, 359–366.
37 D. Vione, G. Falletti, V. Maurino, C. Minero, E. Pelizzetti, M. Malandrino, R. Ajassa, R. Olariu and C. Arsene, *Environ. Sci. Technol.*, 2006, **40**, 3775–3781.
38 J. E. Grebel, J. J. Pignatello and W. A. Mitcha, *Water Res.*, 2011, **45**(19), 6535–6544.
39 R. G. Zepp, *Environ. Sci. Technol.*, 1978, **12**, 327–329.